Photon Recycling and Efficiency Limit of a Silicon Solar Cell with Lambertian Surfaces

by

© *Faezeh Aliabadi Farahani*

A thesis submitted to the

School of Graduate Studies

in partial fulfilment of the

requirements for the degree of

Master of *Science* in Physics

Department of *Physics and Physical Oceanography*

Memorial University of Newfoundland

August 2023

St. John's Newfoundland

Abstract

This thesis introduces an idealized silicon solar cell with Lambertian front and back surfaces. We assume that the reflection coefficient of the back surface is 1. When a photon enters the solar cell, it gets refracted by a randomly corrugated front surface and subsequently undergoes random reflections by back and front surfaces until it either gets absorbed or escapes the material with the probability that depends on the material's refractive index. After each reflection event, the angle of photon propagation relative to the normal is randomized with Lambertian distribution.

This thesis is focused on the photons produced in the radiative recombination events inside the cell. An exact analytical expression for the probability of photon reabsorption and recycling in an idealized solar cell with two Lambertian surfaces is derived. The existing approximations are found to agree with the exact formula to within 5 %. The most accurate approximation turned out to be the simplest one that sets the reabsorption probability to the weak-absorption limit of the cell absorptance. The maximal photoconversion efficiency of a silicon solar cell is evaluated to be 29.5 % at the base thickness of 98 μm.

Acknowledgements

I want to express my gratitude and appreciation to everyone who contributed to completing this thesis. Their support, encouragement, and guidance have been instrumental in making this academic endeavor possible.

First and foremost, I am deeply indebted to my thesis advisor, Dr. Mykhaylo Evstigneev, whose expertise, patience, and unwavering commitment to academic excellence have been invaluable throughout this research journey. Your insightful feedback and constructive criticism have challenged me to grow as a researcher and have significantly improved the quality of this work.

I sincerely thank the Department of Physics and Physical Oceanography faculty members for their dedication to providing a stimulating academic environment. The knowledge and skills I have gained from their lectures and discussions have been instrumental in shaping my understanding of the subject matter.

Finally, I am grateful to my friends and family for their unwavering support and encouragement. Their belief in me has been a constant source of motivation, and I am profoundly grateful for their sacrifices and understanding during the time I devoted to this project.

Contents

List of Tables

List of Figures

Chapter 1

Introduction

1.1 Photovoltaic system

Photovoltaic (PV) systems represent an eminent renewable energy technology rooted in the principles of semiconductor physics and the photovoltaic effect. They directly convert incident solar radiation into electrical energy using semiconductor materials, predominantly silicon. When illuminated by sunlight, these solar cells perform photovoltaic conversion, wherein photons with energies exceeding the semiconductor bandgap promote electrons from the valence to the conduction band, generating electron-hole pairs.

The spatial separation of these electron-hole pairs by the built-in electric field of the p-n junction or heterojunction of the solar cell results in a photo-induced

electric current. The photocurrent collection and efficient extraction constitute the foundation of the photovoltaic energy conversion process.

The fundamental unit of the PV system is the solar panel, which consists of multiple interconnected solar cells [1]. Each solar cell comprises a thin semiconductor layer carefully designed with specific doping profiles to establish the desired junction characteristics.

The conversion of the generated direct current (DC) power into alternating current (AC) electricity, the standard form of electrical energy used in power distribution and consumption, necessitates the incorporation of an inverter. The inverter accomplishes this task through pulse-width modulation and other techniques to produce AC output conforming to the requisite voltage and frequency specifications. An assemblage of balance of system (BOS) components is integrated to ensure the reliable and efficient operation of the PV system. These components encompass wiring, junction boxes, protective devices (e.g., fuses, circuit breakers), and monitoring systems. Wiring facilitates the interconnection of solar panels, the inverter, and associated equipment, allowing for the smooth flow of electric current. Junction boxes serve as connection nodes while protecting the solar cell arrays within the panels. Protective devices are essential for safeguarding the system against overcurrent and fault conditions [2] . Monitoring systems, increasingly equipped with data-driven capabilities, enable real-time performance monitoring,

fault detection, and optimization of system parameters. In specific applications, the integration of energy storage systems, often relying on battery technology, enhances the autonomy of the PV system by enabling the storage of surplus electricity during periods of high solar irradiance. This stored energy can be utilized during low sunlight periods or at night, contributing to the stability and continuity of the electricity supply [3] .

The operational configuration of the PV system may entail either grid-tied or off-grid operation. In grid-tied systems, the surplus electricity produced by the PV system can be fed back into the utility grid, with compensation arrangements such as net metering or feed-in tariffs facilitating a symbiotic relationship between the PV system owner and the grid operator [1] .

Ultimately, the efficacy of the PV system is contingent on various factors, including solar irradiance levels, ambient temperature, system design, and the efficiency of solar cells. As a key contributor to sustainable and environmentally conscious energy generation, the PV system continues to experience technological advancements, efficiency improvements, and cost reduction, bolstering its adoption and integration within the global energy landscape.

Wafer-based crystalline silicon solar cells are a prominent and extensively used photovoltaic device in the solar energy sector. These solar cells are characterized by using thin slices of crystalline silicon wafers as an active semiconductor material

[4] .

The fabrication process of wafer-based silicon solar cells involves several essential stages. First, large cylindrical silicon ingots are grown using the Czochralski or Float Zone method. These silicon ingots are then sliced into thin wafers, typically around 150-200 micrometers thick, using wire sawing techniques [5], [4].

After slicing, the surfaces of the silicon wafers undergo treatment to remove impurities and optimize their light absorption capability. Specific impurities are introduced through doping, which creates a p-n junction within the silicon, facilitating the photovoltaic effect. This doping process establishes regions with excess electrons (n-type) and holes (p-type).

Multiple solar cells are interconnected to form a solar module or panel, which can be further integrated into solar arrays for practical applications. Wafer-based silicon solar cells can be further categorized into two main types based on the type of silicon employed. Monocrystalline silicon solar cells are constructed using single-crystal silicon wafers, offering higher efficiency due to their uniform crystal structure and low recombination rate. On the other hand, polycrystalline silicon solar cells are fabricated using multiple silicon crystals, resulting in slightly lower efficiency compared to monocrystalline cells but offering cost-effectiveness, making them popular for residential and commercial solar installations [4].

To optimize the extraction of the photogenerated charge carriers, metal contacts

are applied to the silicon wafer's front and back surfaces. The front surface, directly exposed to sunlight, may undergo texturing to reduce reflection losses and enhance light absorption. Anti-reflective coatings are also commonly employed to enhance solar cells' light-harvesting capabilities further. In operation, incident photons with energies greater than the silicon bandgap impart sufficient energy to electrons, promoting them across the p-n junction and creating electron-hole pairs. The built-in electric field within the p-n junction then facilitates the separation of these charge carriers, directing electrons toward the n-type region and holes toward the p-type region. This spatial separation gives rise to the photocurrent, constituting the fundamental basis for generating electrical power within the solar cell [4] .

As the demand for sustainable and renewable energy sources intensifies, research and development efforts are ongoing to further enhance the efficiency of wafer-based silicon solar cells. Innovations in material quality, advanced cell architectures, and manufacturing techniques hold the potential to optimize their performance further and contribute to their continued prominence in the global pursuit of clean and renewable energy.

The limit efficiency of single-junction solar cells is a prominent scientific subject, garnering substantial interest due to its relevance in assessing such devices' maximum achievable energy conversion efficiency. This concept encapsulates the

theoretical upper bound on the efficiency of a solar cell utilizing a single semiconductor material [6]. Scientific investigations into the limiting efficiency involve a comprehensive exploration of the fundamental processes governing energy conversion within the device. Key factors under scrutiny include the absorption of incident photons, the conversion of absorbed light into charge carriers, and the subsequent extraction of these carriers to generate electrical current.

Detailed analyses encompass the examination of thermodynamic limits, radiative and non-radiative recombination mechanisms, and the impact of material properties, such as the bandgap and mobility [7]. Furthermore, sophisticated theoretical models and numerical simulations contribute to understanding carrier dynamics, light trapping strategies, and optimizing device architecture. By delving into the scientific intricacies surrounding the limiting efficiency of single-junction solar cells, researchers aim to unravel fundamental principles, identify performance bottlenecks, and drive advancements toward achieving higher energy conversion efficiencies in solar cell technologies.

Maximizing the efficiency of solar cells constitutes a paramount research endeavor within the scientific community, as it holds profound implications for the advancement and widespread adoption of photovoltaic technologies. This pursuit necessitates a multidimensional approach encompassing materials engineering, device physics, and system-level optimization. Scientific investigations into max-

imizing solar cell efficiency involve meticulously exploring various fundamental processes governing light absorption, charge carrier generation, and extraction. Researchers scrutinize the bandgap engineering of semiconductor materials, exploring novel materials, multi-junction configurations, and thin-film technologies to enhance the utilization of a broad spectrum of incident photons [8] . Advanced strategies for light management, such as nanostructuring, photon trapping, and anti-reflection coatings, are pursued to optimize light absorption within the active layer.

Additionally, meticulous attention is paid to reducing energy losses due to recombination, employing surface passivation techniques, defect mitigation strategies, and innovative contact designs. Moreover, optimizing charge carrier transport and extraction through efficient charge collection architectures, carrier mobility enhancement, and electrode engineering is paramount [9]. Researchers also harness advanced modeling, simulation, and optimization techniques to explore optimal device architectures, system-level integration, and energy conversion optimization under diverse operating conditions. Through rigorous scientific inquiry, researchers endeavor to push the boundaries of solar cell efficiency to realize high-performance, economically viable solar energy conversion technologies to sustainably meet the escalating global energy demands.

1.2 Recombination Processes

The recombination process in semiconductors is a fundamental phenomenon that significantly impacts the behavior and performance of electronic devices. It involves the annihilation of charge carriers, namely electrons, and holes, leading to the release of energy. The understanding and control of recombination mechanisms are of paramount importance in semiconductor physics and device engineering.

Recombination is an elementary process occurring in semiconductors, wherein a conduction electron reoccupies an empty state in the valence band, creating what is known as a hole [10]. Conservation of energy and momentum is crucial during electron-hole recombination. Notably, most conduction electrons occupy states near the bottom of the conduction bands, while most holes are localized near the top of the valence band. Consequently, the energy released during recombination is approximately equivalent to the bandgap energy, denoted as E_g. The momentum released in a recombination event depends on the semiconductor's intrinsic characteristics. In direct-bandgap semiconductors, the conduction band's bottom aligns with the valence band's top in momentum space, releasing no momentum during recombination.

Recombination can occur through various channels, including radiative recombination, where photons are emitted, and non-radiative recombination, which in-

volves energy dissipation without photon emission [10]. Intrinsic recombination processes, such as radiative and Auger recombination, are inherent to the semiconductor material. Extrinsic recombination processes, such as surface recombination and impurity- assisted Shockley-Read-Hall mechanism are influenced by external factors such as interfaces and impurities [11].

Additionally, defects play a crucial role in modifying the recombination kinetics. A comprehensive understanding of recombination processes is essential for optimizing carrier lifetime and minimizing losses, thereby enhancing the performance of semiconductor devices.

Radiative recombination is a process, in which a photon is emitted [12]. Due to energy conservation, the energy disparity between the electron and hole states equals the photon energy. Radiative recombination is more relevant in direct-bandgap semiconductors, wherein the electron and hole states overlap in the momentum space [10, 13]. This overlap facilitates a favorable coupling of the electron and hole wavefunctions, thereby augmenting the probability of radiative recombination. The radiative recombination process's ramifications are instrumental in optoelectronic devices, including light-emitting diodes and lasers, wherein the generation of photons constitutes a core objective [14]. Hence, comprehending and governing radiative recombination mechanisms' intricacies are indispensable for optimizing these devices. To this end, diverse strategies encompassing mate-

rial engineering, defect management, and interface design are employed [15]. In the indirect-bandgap semiconductors, including silicon, radiative recombination proceeds about $10^4 - 10^5$ time more slowly than in the direct-bandgap semiconductors.

Auger recombination proceeds via concurrent interaction of three charge carriers, either two electrons and a hole or two holes and an electron [16]. Differing from radiative recombination, Auger recombination does not involve the emission of photons. Instead, it entails the transfer of excess energy from one carrier to another, generating a high-energy carrier. Auger recombination can significantly impede the overall efficiency of semiconductor devices, as the excess energy is dissipated as heat rather than light emission. Multiple factors, including carrier concentrations, doping levels, and the availability of energy states within the band structure, influence the rate of Auger recombination [17]. A comprehensive understanding and meticulous control of Auger recombination are of utmost importance for enhancing the performance of semiconductor devices and minimizing non-radiative losses. Consequently, a range of strategies encompassing bandgap engineering, defect management, and material optimization are pursued to effectively mitigate Auger recombination and enhance the overall efficiency of semiconductor devices.

Trap-assisted Shockley-Read-Hall (SRH) recombination is a prominent non-

radiative recombination process observed in semiconductors, wherein traps significantly influence the carrier recombination dynamics. This phenomenon occurs when a charge carrier is captured by a trap – an impurity atom whose energy level happens to be approximately in the middle of the bandgap [16]. The captured carrier becomes immobile. Subsequently, a recombination event occurs when another charge carrier of opposite polarity encounters the trap. The rate of trap-assisted SRH recombination depends on several factors, including trap densities, trap energy levels, and carrier concentrations.

Finally, surface recombination is a consequential phenomenon in semiconductors that occurs at the interfaces between the semiconductor material and its surrounding environment. Surface recombination is primarily caused by surface states, defects, and impurities that act as recombination centers, facilitating the annihilation of charge carriers. As charge carriers approach the surface, they encounter these surface recombination centers, resulting in their capture and subsequent recombination. This process negatively impacts the efficiency and performance of semiconductor devices, particularly in applications where high carrier lifetimes are desired. Therefore, understanding and controlling surface recombination mechanisms are crucial for optimizing device performance [18]. Techniques such as surface passivation, surface cleaning, and interface engineering are employed to reduce surface recombination rates and enhance carrier lifetime, ultimately im-

proving the overall efficiency of semiconductor devices.

1.3 Objectives

Technological progress in semiconductor processing has brought about a transformative capability: the production of crystalline silicon distinguished by significantly extended charge carrier lifetimes [19–21] and notably reduced surface recombination velocity [19, 22–26]. This has shown in a new era where silicon solar cells can achieve efficiencies surpassing 20%, with some even achieving a remarkable 26% and beyond [27, 28].

Within this context of advanced solar cells, the fundamental limit on efficiency lies in intrinsic radiative and Auger recombination mechanisms. Radiative recombination takes precedence, especially when excess carrier concentrations dip below roughly $10^{15}\,\mathrm{cm}^{-3}$, a range commonly observed near the point of maximal power output in an ideal solar cell. It is important to note that radiative recombination differs from Auger recombination in reversibility. Specifically, photons generated during radiative recombination events can be reabsorbed by the semiconductor material, creating new electron-hole pairs, a phenomenon known as "photon recycling."

Various approximations have been proposed to quantify the probability of pho-

ton reabsorption within these solar cells. As documented in prior research [29, 30], the most straightforward approach involves equating this probability with absorptance, representing the probability of a photon entering the material from an external source being absorbed. Nevertheless, it is imperative to acknowledge that this approximation overlooks the potential variation in absorption probability contingent upon the photon's position within the cell at the moment of generation. Such simplifications remain valid under specific conditions, notably when $\alpha L \ll 1$, where α signifies the absorption coefficient and L denotes the thickness of the cell. Recent developments have yielded a more refined approximate formula [31], which accounts for the spatial distribution of photon generation within the solar cell.

This thesis gives a detailed account of the result reported in the joint publication [32] by the author and her research supervisor. While the main result of [32], namely, the photon reabsorption probability, was derived by Dr. Evstigneev, the author of this thesis has confirmed its correctness by performing a numerical experiment using the ray tracing technique, applied it to calculate the limit efficiency of a silicon solar cell, and participated in the write-up of the paper.

The thesis embarks on a comprehensive exploration of photon recycling probability within an idealized solar cell distinguished by Lambertian front and back surfaces. It involves a comparative analysis of the prevailing approximations [29–

31] and the exact results. Ultimately, this examination reveals that the simplest approximation outlined in [29] provides the most precise depiction of photon re-absorption. Subsequently, the exact formula is applied to ascertain the limiting efficiency of silicon solar cells, and the findings indicate a remarkable efficiency of 29.5% when the cell has a thickness of 97.6 μm.

Chapter 2

Absorptance and reabsorption probability for Lambertian front and back surfaces

2.1 Introduction

Surface reflection can be broadly categorized into four types: diffuse, glossy specular, perfect specular, and retro-reflective. Most real surfaces display a combination of these four types [33]. Diffuse surfaces scatter light uniformly in all directions. While having an utterly diffuse surface is impossible, some surfaces, like dull chalkboards and matte paint, come quite close to it. Conversely, glossy spec-

ular surfaces, including high-gloss paint and plastic, reflect light in specific preferred directions, which causes surrounding objects to have blurred reflections. Perfect specular surfaces reflect light in only one direction, with mirrors and glass as prime examples. Retro-reflective surfaces, such as velvet and the moon's surface, scatter light primarily in the same direction it came from.

The traditional way of representing how surfaces reflect light assumes that tiny, uniform facets are scattered in all directions [34]. This uniform distribution of facets serves to randomize the direction of reflected light, resulting in a consistent isotropic behavior. However, some surfaces have a specific directional pattern, such as those created by sanding or machining. These surfaces exhibit anisotropic lighting properties. Even though the facets or grooves are not visible to the naked eye, their effect on the lighting is noticeable. Some everyday objects that display anisotropic lighting are CDs and vinyl records.

In the next section of this chapter, ideally diffusive Lambertian reflection is explained together with its use to trap light by a solar cell. Then, absorptance in a solar cell with Lambertian front and back surfaces is discussed. Finally, an analytical expression for the probability of reabsorption of photons produced in radiative recombination events is derived in the last section, which is taken with minimal modifications from the recently published paper [32].

2.2 Lambertian Light Trapping

2.2.1 Lambertian Reflection of Light

Lambertian reflection of light, a well-known phenomenon studied within optics, has garnered substantial scientific attention owing to its broad applicability in various fields, including lighting, imaging, and solar energy conversion. This phenomenon describes the diffuse light reflected by a surface that exhibits ideal Lambertian behavior. Lambertian reflection is characterized by the property of isotropy, where incident light is scattered uniformly in all directions, regardless of the angle of incidence. Scientific investigations into Lambertian reflection encompass a comprehensive exploration of the underlying physical mechanisms governing light scattering by microstructural and macrostructural features of a surface[35].

Studying the Lambertian reflection extends to understanding the impact of surface roughness, material properties, and environmental factors on scattering behavior, thereby enabling the design and optimization of optical systems, light extraction strategies, and solar concentrators. Theoretical models based on radiative transfer theory and scattering theories, such as Mie theory or Rayleigh scattering, are employed to analyze and predict the intensity and angular distribution of the reflected light.

Consider a system where a flux of photons, represented by j, hits a rough sur-

face. Due to the roughness of the surface, the photons scatter randomly in all directions with an equal probability. If we take a small circular area on the surface, denoted as ΔA_0, it will scatter $\Delta I_0 = j\Delta A_0$ photons per unit of time into a solid angle of 2π, which corresponds to a hemisphere. The angle between the surface normal that goes through the center of ΔA_0 and the scattering direction is represented by θ. If the surface element is viewed from an angle θ, its apparent area equals $\Delta A(\theta) = \Delta A_0 \cos(\theta)$. At large distances, this surface element appears as a point-like intensity source proportional to $\Delta A(\theta)$:

$$\Delta I(\theta) = j\Delta A_0 \cos(\theta) = \Delta I_0 \cos(\theta) \tag{2.1}$$

independent of the angle of incidence. This is Lambert's cosine law. The probability for a photon to be reflected at an angle between θ and $\theta + d\theta$ is proportional to $\Delta I(\theta)$, and the solid angle $d\Omega = 2\pi \sin(\theta) d\theta$:

$$f(\theta) = 2\sin(\theta)\cos(\theta) = \sin(2\theta) \tag{2.2}$$

where factor 2 follows from the normalization condition $\int_0^{\pi/2} f(\theta)\, d\theta = 1$.

2.3 Absorptance

Absorptance quantifies the efficacy with which a material absorbs incident electromagnetic radiation. In classical electromagnetism, absorptance measures the

fraction of power absorbed by a material relative to the incident power [36]. It is determined by the complex refractive index of the material, which incorporates both the real part representing the refractive properties and the imaginary part associated with absorption. The interaction of electromagnetic waves with a material gives rise to various absorption mechanisms, including electronic transitions, vibrational modes, and lattice excitations.

2.3.1 Absorptance Near the Absorption Edge

The absorption edge denotes the wavelength range at which a semiconductor material experiences a substantial increase in light absorption. This region corresponds to energy levels near the bandgap, where optical transitions occur, leading to the excitation of electrons from the valence band to the conduction band.

The absorption coefficient quantifies the photon absorption probability per unit path length. In the vicinity of the absorption edge, the absorption coefficient exhibits a steep rise due to the increased availability of electronic states for absorption, resulting in enhanced light harvesting capabilities [37]. The density of states within the conduction and valence bands and the presence of defects and impurities in the material also affect the absorptance behavior. Understanding and optimizing the absorptance characteristics near the absorption edge are crucial for developing solar cells with improved performance and increased energy conver-

sion efficiency.

Various material parameters govern the absorptance characteristics of solar cells near the absorption edge. The bandgap width of the semiconductor material plays a critical role in determining the absorptance behavior. A narrower bandgap shifts the absorption edge to longer wavelengths, allowing for the absorption of higher energy photons and thereby enhancing the overall absorptance in this spectral region [38].

Furthermore, the thickness of the absorber layer in the solar cell structure impacts the absorptance near the absorption edge. A thicker absorber layer allows for a higher probability of photon absorption, resulting in enhanced light absorption efficiency. By precisely controlling these material parameters, the absorptance near the absorption edge can be optimized, leading to improved solar cell performance and increased solar energy conversion efficiency.

Outlined below is the derivation of an asymptotic formula described in the reference [39]. The subject of study is a semiconductor slab with a thickness of L and two rough surfaces. The front surface is treated so that all incident photons at a normal angle enter the material, and their direction of propagation is immediately randomized upon refraction. The reflection of both surfaces is assumed to be Lambertian, with the back surface having a reflection coefficient of 1 and the front

surface reflecting photons incident at an angle higher than the critical angle [39]

$$\theta_c = \sin^{-1} n_r^{-1} \tag{2.3}$$

relative to the local normal to the surface. If the front surface were flat, then photons with an angle of incidence $\theta < \theta_c$ escape the material, whereas the photons incident at an angle $\theta > \theta_c$ undergo total internal reflection with the angle or reflection equal the angle of incidence.

For a corrugated surface, photon escape and reflection are random events, for which only the probabilities can be defined. Furthermore, if the photon gets reflected, its angle of reflection is characterized by the Lambertian probability distribution (2.2) independent of the angle of incidence. It is postulated that the probability for a photon to escape is obtained by integrating this distribution from zero to the critical angle [39, 40]:

$$p_e = \int_0^{\theta_c} \sin(2\theta)\, d\theta \; = n_r^{-2} \tag{2.4}$$

The average distance traveled by a photon before two successive contacts with the front surface is

$$\langle l \rangle = 2 \int_0^{\pi/2} f(\theta) \frac{L}{\cos\theta} d\theta \; = 4L \int_0^{\pi/2} \sin\theta \, d\theta = 4L \tag{2.5}$$

Near the absorption edge, where the energy of a photon hf only slightly exceeds to the bandgap energy E_g, the photon moves back and forth between two surfaces

multiple times before being absorbed or escaping. The coefficient for band-to-band absorption is labeled as α_b, while the coefficient for parasitic absorption, that part of the incident sunlight absorbed by the device does not contribute to the obtainable photocurrent, is labeled as α_p. Additionally, the escape coefficient, which is the probability of a photon escaping per unit path length, can be introduced:

$$\alpha_e = \frac{p_e}{\langle l \rangle} = \frac{1}{4Ln_r^2} \tag{2.6}$$

The absorptance is defined as the probability for a photon that entered the material to be absorbed with the generation of an electron-hole pair:

$$A_b = \frac{\alpha}{\alpha + \alpha_e} \tag{2.7}$$

In this limit with $\alpha = \alpha_b + \alpha_p$ and α_e given by the expression above, we obtain the Tiedje-Yablonovitch formula [39]

$$A = \frac{1}{1 + \dfrac{1}{4\alpha Ln_r^2}} \tag{2.8}$$

2.3.2 Absorptance for Lambertian Front and Back Surfaces

The scattering of incident photons by a Lambertian surface occurs in a manner that increases the optical path length within the absorber layer. This enhances the absorption probability, improving light harvesting capabilities. The diffuse

scattering also reduces the reflectance from the front surface, minimizing the loss of incident photons.

This phenomenon is especially relevant for thin-film solar cells, where the absorption path is typically shorter. The diffuse scattering at the back surface enhances the absorption of photons that would otherwise escape the device, increasing the overall absorptance [41]. Therefore, a comprehensive understanding of the absorptance behavior for Lambertian front and back surfaces is crucial for designing and optimizing solar cells to maximize light absorption and improve device performance.

Here, we obtain a general equation for the absorptance of a semiconductor slab with two irregular surfaces by referring to [42] . We define T_L as the probability of a photon passing from one surface to another without absorption. After entering the material, the probability for a photon not be absorbed is

$$1 - A = T_L^2 p_e + T_L^2 (1 - p_e) T_L^2 p_e + T_L^2 (1 - p_e) T_L^2 (1 - p_e) T_L^2 p_e + \cdots . \tag{2.9}$$

The initial term denotes the probability of escaping after making a round trip, then traveling back and escaping again. The second term indicates the probability of escaping after two round trips, and so on. By recognizing that this is the sum of a geometric series, we can simplify the equation to:

$$1 - A = \frac{T_L^2 p_e}{1 - T_L^2 (1 - p_e)} \tag{2.10}$$

and from Equation (2.4) absorptance is

$$A = \frac{1 - T_L^2}{1 - T_L^2(1 - n_r^{-2})} \tag{2.11}$$

The probability of traveling from one surface to the other without absorption is

$$T_L = \int_0^{\pi/2} f(\theta) e^{-\alpha L/cos\theta} d\theta \; = 2 \int_0^1 c e^{-\alpha L/c} dc \tag{2.12}$$

where we used Lambertian expression from Equation (2.4) and changed the integration variable to $c = cos\theta$. Employing a different variable for integration $x = \alpha L/c$ we have

$$\begin{aligned} T_L &= 2(\alpha L)^2 \int_{\alpha L}^{\infty} \frac{e^{-x}}{x^3} dx \; = -(\alpha L)^2 \int_{\alpha L}^{\infty} e^{-x} \frac{d}{dx} \frac{1}{x^2} dx \\ &= -(\alpha L)^2 \left(\frac{e^{-\alpha L}}{(\alpha L)^2} + \int_{\alpha L}^{\infty} \frac{e^{-x}}{x^2} dx \right) \end{aligned} \tag{2.13}$$

We have performed integration by parts. Performing another integration by parts [43], we obtain

$$T_L = (\alpha L)^2 E_1(\alpha L) + (1 - \alpha L) e^{-\alpha L} \tag{2.14}$$

where

$$E_1(x) = \int_x^{\infty} \frac{e^{-t}}{x} dt \tag{2.15}$$

is the exponential integral.

The probability of absorption with a generation of an electron-hole pair is

$$A_b = \frac{\alpha_b}{\alpha_b + \alpha_p} A \tag{2.16}$$

2.4 Photon reabsorption probability

Let us discuss the photons generated during the radiative recombination process. Right after recombination, the resulting photon has a uniform distribution of angles in all directions.

$$f_i(\theta) = \frac{1}{2} \sin\theta \quad 0 < \theta < \pi \tag{2.17}$$

The angle θ is calculated relative to the perpendicular line of the rear surface. The newly formed photon can either be reabsorbed or it may eventually escape, with a probability of $P_{esc} = 1 - P_{reabs}$.

Consider the photons produced at a distance $x > 0$ from the front surface in the $x = 0$ plane. Among those photons, half travel towards the front surface and half towards the back surface. The chance of reaching front surface without being absorbed is considered for photons traveling toward the front surface.

For those photons which propagate toward the front surface, the probability of reaching it without absorption is

$$\int_0^{\pi/2} f_i(\theta) e^{-\alpha x/\cos\theta} d\theta \; = \frac{1}{2} \int_0^1 e^{-\alpha x/c} dc \; , \tag{2.18}$$

where we changed the integration variable to $c = \cos\theta$. Assuming that photons are created uniformly throughout the material, we can calculate the average probability of a photon generated through radiative recombination reach the front surface:

$$\begin{aligned} P_1 = \frac{1}{2}\int_0^L \frac{dx}{L}\int_0^1 e^{-\alpha x/c}dc &= \frac{1}{2\alpha L}\int_0^1 c(1-e^{-\alpha x/c})dc \\ &= \frac{1}{2\alpha L}\left(\frac{1}{2} - \int_0^1 ce^{-\alpha x/c}\,dc\right) \end{aligned} \tag{2.19}$$

The integral in the brackets appears in Equation (2.13) and has the value of $T_L/2$. Thus

$$P_1 = \frac{1-T_L}{4\alpha L} \tag{2.20}$$

Dissecting limiting weak and strong absorption cases is helpful to understand this statement better. When a photon travels between two surfaces, the probability of it passing through in the case of weak absorption is

$$T_L \approx e^{-2\alpha L} = 1 - 2\alpha L + \cdots \tag{2.21}$$

And thus, $P_1 = 1/2$ is in the leading order of αL. Indeed, without absorption, a photon produced in a recombination event reaches either surface with the probability of $1/2$.

Now let us discuss the converse scenario of strong absorption, where αL is greater than 1. When a photon is produced at a distance x from the surface and

moves at an angle θ, it must travel a distance of $x/\cos(\theta)$ to reach the surface. Considering the isotropic angular distribution described in Equation (2.17), we can determine the proportion of photons that manage to escape

$$\int_0^{1/\alpha} \frac{dx}{L} \int_0^{cos^{-1}(\alpha x)} f_i(\theta)\, d\theta \; = \frac{1}{4\alpha L} \tag{2.22}$$

The same result is obtained from Equation (2.20) with T_L set to 0.

Next, let us focus on the photons that are moving in the direction of the back surface. These photons have the same probability of reaching the back surface as the previous ones, P_1. Once they reach the back surface, they bounce off it, and their angular distribution changes from isotropic (as described in Equation (2.17)) to Lambertian (as defined in Equation (2.2)). Then, the photons have a probability of T_L reaching the front surface. Therefore, the probability that a photon reaches the front surface after being reflected by the back surface is given by

$$P_2 = P_1 T_L \tag{2.23}$$

The probability for a newly created photon to reach the front surface via either of these routes is

$$P_f = P_1 + P_2 = P_1(1 + T_L) = \frac{1 - T_L^2}{4\alpha L} \tag{2.24}$$

Once the photon reaches the front surface, there are two possible outcomes: it can either escape with the probability of p_e or be reflected with the probability of

$1 - p_e$. In the latter case, the photon still has a chance to escape the material with the probability of $1 - A$, where A is the absorptance of the material as defined in Equation (2.11). Therefore, we can calculate the reabsorption probability by subtracting the escape probability from 1

$$P_{esc} = P_f p_e + P_f (1 - p_e)(1 - A) \tag{2.25}$$

After a straightforward algebra, we obtain the probability of photon reabsorption using Equation (2.4) and Equation (2.11).

$$P_{reabs} = 1 - P_{esc} = 1 - \frac{1 - T_L^2}{4\alpha L(n_r^2 - T_L^2(n_r^2 - 1))} \tag{2.26}$$

This is the main result of this thesis [32].

To ensure complete accuracy, we confirmed the validity of Equation (2.26) by running Monte Carlo simulations on a vast number of photons (10^8) that were uniformly generated between 0 and L using the method outlined in reference [44]. Across all tested parameters, we determined the reabsorption probability by calculating the fraction of photons that failed to exit the semiconductor slab. This numerical result aligned with the value predicted by Equation (2.26) within the statistical margin of error in the simulations. Any dissimilarities between the numerical and theoretical results were minimal, at approximately 0.1%.

Chapter 3

Solar cell limit efficiency

3.1 Introduction

Because silicon is the most popular material from which solar cells are made, determination of their maximal possible efficiency is an important research question which has been pursued in a number of papers [29, 30, 39, 44–47]. These calculations are based on the model, in which 100 % of the incident sunlight enters the cell (i.e. no reflection by the front surface), only intrinsic recombination mechanisms are operative, and the effects of the parasitic series and shunt resistance are neglected. Since intrinsic recombination is minimized if the concentrations of electrons and holes are equal, the cell material must be intrinsic rather than doped silicon. For this reason, the next section of this chapter briefly recalls the properties

of the intrinsic semiconductors. Next, the derivation of the radiative recombination coefficient in a semiconductor based on the seminal work by Peter Würfel [48]. In the next section, which is taken from the author's earlier publication [32], the analytical result for photon reabsorption probability is compared with the approximate expressions found in the literature. Finally, following the same work [32], the new efficiency limit of a silicon solar cell is established in the concluding section of this chapter.

3.2 Intrinsic Semiconductors

A semiconductor is a material with an innate ability to conduct electricity, even to a limited extent, due to thermally generated charge carriers. Unlike extrinsic semiconductors intentionally doped with impurities to enhance their conductivity, intrinsic semiconductors exhibit a natural balance between electrons and holes in thermal equilibrium. In this state, the Fermi level resides at the center of the energy band gap, resulting in a relatively low electrical conductivity. The intrinsic semiconductors' fundamental properties are governed by energy band structure, carrier mobility, and recombination processes. Understanding the intricacies of intrinsic semiconductors is paramount in various fields, including solid-state physics, electronics, and semiconductor device engineering.

Charge carriers refer to entities, such as electrons or electron deficiencies (holes), that possess an electric charge and are responsible for the conduction of electricity in materials. These carriers can move through a material in response to an applied electric field, thereby contributing to the flow of electric current. In the case of metals, the charge carriers are electrons detached from their parent atoms and capable of moving freely throughout the material.

In contrast, semiconductors' charge carriers can be electrons and holes. Electrons, as negatively charged carriers, contribute to the current by their motion, while holes, representing the absence of an electron in an otherwise filled electron state, behave as positively charged carriers and drift in the opposite direction.

The Fermi level signifies the energy level where all electronic states are occupied by electrons below it, while states above it remain unoccupied at absolute zero temperature. The Fermi level plays a critical role in determining materials' electrical and thermal properties, especially in semiconductors and metals, as it dictates the distribution of electrons and their availability for conduction. Additionally, the position of the Fermi level relative to the energy band structure influences phenomena such as carrier concentration, electrical conductivity, and formation of energy barriers and junctions in electronic devices. Understanding and controlling the Fermi level is essential for designing and optimizing the performance of electronic devices and materials in various scientific and technological applications.

3.3 The effective radiative recombination coefficient

We now consider an idealized solar cell with the non-equilibrium electron and hole concentrations, n and p, uniformly distributed within the cell volume. In a non-degenerate semiconductor, they are related by the generalized mass action law

$$np = n_i^2(V)\, e^{qV/kT} \tag{3.1}$$

in which V is the voltage across the cell, q is the elementary charge, and kT is the thermal energy. The intrinsic concentration n_i is corrected with respect to the bandgap narrowing effect [49],

$$n_i(V) = n_{i0} e^{\Delta E_g(V)/(2kT)}\ , \tag{3.2}$$

where n_{i0} is the carrier concentration in an undoped semiconductor at zero excitation level and $\Delta E_g(V)$ is the size of bandgap narrowing that depends on the voltage via the carrier concentrations $n(V)$ and $p(V)$ [49]. Together with the charge neutrality condition,

$$n + N_a = p + N_d\ , \tag{3.3}$$

in which $N_{a,d}$ are the concentrations of the ionized acceptors and donors, Equation (3.1) and Equation (3.2) allow to numerically determine the carrier concentrations $n(V)$, $p(V)$ and the effective intrinsic concentration $n_i(V)$.

When a semiconductor device operates, it deviates from a state of equilibrium. It experiences the flow of electric current caused by various factors, such as an

applied electric field or the generation of electron-hole pairs due to incident solar radiation [10].

Fortunately, in most practical scenarios, when a semiconductor device is not in equilibrium, the changes in its macroscopic parameters, such as temperature, chemical potential, and electric field, tend to be gradual across space. This allows us to divide the semiconductor into small elements of volume dV mentally. Each element can be considered a system that closely approximates thermodynamic equilibrium. Each element is characterized by its quantities, including the number of electrons and holes (dN_e and dN_h), energy levels E, and Fermi energy E_F [10].

Assuming that the small volume dV is centered around a generic point $\vec{r}$, we can define the local density of electrons and holes as $n(\vec{r}) = dN_e/dV$ and $p(\vec{r}) = dN_h/dV$.

When a semiconductor is subjected to non-equilibrium conditions caused by an external disturbance, such as an electric field, and that disturbance is subsequently turned off, the system begins a process of equilibration until it returns to equilibrium. The restoration of equilibrium occurs through various mechanisms, including the lattice's scattering of electrons and holes and collisions between electrons and holes. Additionally, there are generation processes in which electron-hole pairs are created due to the promotion of electrons from the valence band to

the conduction band and recombination processes where electron-hole pairs are mutually annihilated.

Each of these processes exhibits its special rate. Typically, the equilibration of electrons within the same band, either valence or conduction, occurs much more rapidly than achieving a balance between electrons from different bands. The attainment of equilibrium between electrons and holes happens significantly slower than the equilibration processes occurring independently within the electron and hole subsystems.

Therefore, Fermi-Dirac equations can describe the probability distributions of electrons and holes within a specific small volume dV.

$$f_e(E) = \frac{1}{1 + e^{(E - E_{F_e})/kT}} \quad , \quad f_h(E) = \frac{1}{1 + e^{(E_{F_h} - E)/kT}} \tag{3.4}$$

be the probabilities for a state with the energy E in the conduction and valence bands, respectively, to be occupied by an electron or a hole.

The concentration of particles is closely linked to the respective Fermi energy [10]. Consequently, we can deduce that the electron and hole subsystems must possess distinct Fermi energies, referred to as E_{Fe} for electrons and E_{Fh} for holes.

Up to notational differences, the treatment here follows [48].

3.3.1 Einstein's Coefficients

Einstein's coefficients are a paramount theoretical construct in quantum mechanics. They constitute a fundamental framework that enables a profound comprehension of radiative transitions occurring in atoms and molecules, specifically regarding their interaction with light.

Absorption enables an atom to transition from its ground state to an excited state; a photon with a frequency f transfers its energy hf. This transfer can only occur if the photon's frequency precisely matches the excitation energy divided by Planck's constant [50].

$$f = \Delta E/h = (E_2 - E_1)/h \tag{3.5}$$

An atom cannot be excited by a photon with a frequency lower than this value because of energy conservation. On the other hand, it needs to be clarified why a photon with a frequency higher than $\Delta E/h$ cannot transfer a portion of its energy to an atom. This limitation is related to the particle nature of photons. As particles, photons cannot be partially absorbed; they can only be either fully absorbed or not absorbed at all.

Spontaneous emission is a process in which an excited atom reverts to its ground state by releasing a photon with energy $hf = E$. This emitted photon travels in a random direction.

Spontaneous emission arises from the inherently probabilistic nature of quantum mechanics. When an atom or molecule in an excited state undergoes spontaneous emission, it transitions to a lower energy state by releasing a photon without external stimulation [50]. This process occurs independently of incident photons or external fields, distinct from stimulated processes. Einstein's Coefficient here quantifies the rate at which spontaneous emission occurs.

Stimulated emission refers to a process where an excited atom transitions to its ground state upon being exposed to an incoming photon while simultaneously emitting an additional photon. For this process to proceed, it is necessary for the incident and emitted photon to have nearly identical frequencies, very close to the value of $\Delta E/h$, where ΔE represents the energy difference between the excited and ground state of the atom. Following a stimulated emission, the initial photon does not vanish, resulting in the presence of two photons. Each of these photons has the potential to induce another emission event, leading to a total of four photons, then eight photons, and so on [50]. The number of photons may increase rapidly, resembling an avalanche effect. An essential aspect of stimulated emission is that all the generated photons move in the same direction. This characteristic lies at the core of the principle of lasing.

Stimulated emission results from the delicate interplay between photons and quantum systems. When an atom or molecule in an excited state is stimulated by

an external photon that matches the energy level spacing of the transition, it undergoes a transition to a lower energy state while emitting a photon identical to the stimulating photon. This process fundamentally differs from spontaneous emission, as it is triggered by an external photon rather than spontaneously occurring [50].

The significance of Einstein's Coefficients is not confined to theoretical constructs; they find wide-ranging applications in diverse scientific disciplines and practical technologies. In laser physics, the principles of stimulated emission are fundamental to the operation of lasers, enabling the production of coherent and highly amplified light beams. Furthermore, in astrophysics, these coefficients are indispensable in analyzing radiative processes occurring in stars and interstellar media, shedding light on the intricate behavior of celestial objects. Additionally, in the burgeoning domain of quantum optics, Einstein's Coefficients hold profound implications, allowing for a comprehensive description of light-matter interactions at the quantum level and offering promising avenues for quantum information processing and communication technologies.

The densities of states $g_C(E)$ and $g_V(E)$ give the concentration of electron and hole spin and momentum states per unit energy interval [48]. Hence, the concentrations of electrons and holes are

$$n(E) = g_C(E) f_e(E) \quad , \quad p(E) = g_V(E) f_h(E) \tag{3.6}$$

They change in time due to photon absorption, spontaneous emission, and stimulated emission. The respective rates of these processes are

$$\left(\frac{dn(E+hf)}{dt}\right)_{abs} = A(E,f)\rho(f)g_V(E)(1-f_h(E))g_C(E+hf)\times\cdots \\ \cdots(1-f_e(E+hf)) \tag{3.7}$$

$$\left(\frac{dn(E+hf)}{dt}\right)_{spon} = -B(E,f)g_V(E)f_h(E)g_C(E+hf)f_e(E+hf) \tag{3.8}$$

$$\left(\frac{dn(E+hf)}{dt}\right)_{stim} = -C(E,f)\rho(f)g_V(E)f_h(E)g_C(E+hf)f_e(E+hf) \tag{3.9}$$

In this context, "spectral concentration," denoted by $\rho(f)$, refers to the photons at a specific frequency f. The parameter $A(E,f) > 0$ is the probability of photon absorption by an atom per unit time. The parameter $B(E,f)$ is the probability of photon absorption by an atom per unit time. The physical meaning of the parameter $C(E,f)$ is the probability for the emission to be stimulated by a single photon per unit time. The values $A(E,f)$, $B(E,f)$, and $C(E,f)$ are called Einstein's coefficients and determined by both the energy and frequency but not by the electron and hole statistics. Their dimensions are

$$[A(E,f)] = [B(E,f)] = [C(E,f)] = s^{-1} \tag{3.10}$$

More importantly, the occupation probability combinations that determine the rates of spontaneous and stimulated emission are the same. Regarding the absorption rate, the mentioned combination can be expressed as follows.

$$\begin{aligned}(1-f_h(E))(1-f_e(E+hf)) &= \frac{1}{(1+e^{(E-E_{Fh})/kT})(1+e^{-(E+hf-E_{Fe})/kT})} \\ &= \frac{1}{(1+e^{-(E-E_{Fh})/kT})e^{(E-E_{Fh})/kT}(1+e^{-(E+hf-E_{Fe})/kT})} \\ &= \frac{f_h(E)}{e^{(E-E_{Fh})/kT}+e^{-(hf-E_{Fe}+E_{Fh})/kT}} = f_e(E+hf)f_h(E)e^{(hf-q_eV)/kT}\end{aligned} \tag{3.11}$$

where we multiplied the numerator and the denominator with $e^{-(hf-E_{Fe}+E_{Fh})/kT}$ and used the identity

$$E_{Fe} - E_{Fh} = q_eV \tag{3.12}$$

Where q_e is the elementary charge. With this observation and using the definitions of the electron and hole concentrations, the rates can be written as

$$\left(\frac{dn(E+hf)}{dt}\right)_{abs} = A(E,f)\rho(f)p(E)n(E+hf)e^{(hf-q_eV)/kT} \tag{3.13}$$

$$\left(\frac{dn(E+hf)}{dt}\right)_{spon} = -B(E,f)p(E)n(E+hf) \tag{3.14}$$

$$\left(\frac{dn(E+hf)}{dt}\right)_{stim} = -C(E,f)\rho(f)p(E)n(E+hf) \tag{3.15}$$

Consecutively, for the total rate of change of the electron concentration to be zero, the sum of the absorption and the stimulated emission rates must be balanced by the spontaneous emission rate:

$$\left(\frac{dn(E+hf)}{dt}\right)_{abs} + \left(\frac{dn(E+hf)}{dt}\right)_{spon} + \left(\frac{dn(E+hf)}{dt}\right)_{stim} = 0 \tag{3.16}$$

$$\rho(f)(A(E,f)e^{(hf-q_eV)/kT} - C(E,f)) = B(E,f) \tag{3.17}$$

This can only be achieved if

$$A(E,f) = C(E,f) \quad , \quad B(E,f) = A(E,f)g_{ph}(f) \tag{3.18}$$

and

$$\rho(f) = \frac{g_{ph}(f)}{e^{(hf-q_eV)/kT} - 1} \tag{3.19}$$

where $g_{ph}(f)$ is the density of phonon states. In contrast to the standard Planck formula, photons in a semiconductor have a chemical potential of

$$\mu_{ph} = q_eV \tag{3.20}$$

We assume that the material and the photons find themselves in a cube of side length L with periodic boundary conditions. Then, the allowed wave vectors are

$$\vec{k} = \frac{2\pi}{L}\vec{l} \tag{3.21}$$

Where $\vec{l}$ is a vector whose all three components are integers. The number of photon states with the wave number $k = |\vec{k}|$ smaller than a given value in a unit volume is

$$N(k) = 2.\frac{4\pi k^3}{3}.\frac{1}{8\pi^3} = \frac{k^3}{3\pi^2} \tag{3.22}$$

where factor 2 comes from 2 spins allowed for each and $\vec{k}$ and $\frac{1}{8\pi^3}$ is the volume that a state occupies according to Equation (3.21).

The frequency is related to the wave number by

$$k = \frac{2\pi n_r(f)}{c} f \tag{3.23}$$

where $n_r(f)$ is the material's refraction index. Then, the photon density of states is given by

$$g_{ph}(f) = \frac{dN}{dk}\frac{dk}{df} = \frac{8\pi f^2 n_r^3(f)}{c^3}\left(1 + \frac{f}{n_r}\frac{dn_r}{df}\right) \tag{3.24}$$

where the second term in the brackets is neglected in [48].

The absorption coefficient, denoted by $\alpha_b(f)$, represents the probability of a photon being absorbed per unit path length. In a design with only absorption and stimulated emission within the material, the number of photons would decrease at a specific rate over time.

$$\left(\frac{d\rho(f)}{dt}\right)_{abs+stim} = -\int\left(\left(\frac{dn(E+hf)}{dt}\right)_{abs} - \left(\frac{dn(E+hf)}{dt}\right)_{stim}\right)dE \tag{3.25}$$
$$= \alpha_b(f)\rho(f)c_g(f)$$

where the group velocity of light in the material is

$$c_g(f) = \frac{2\pi}{dk/df} = \frac{c}{n_r\left(1 + \frac{f}{n_r}\frac{dn_r}{df}\right)}. \tag{3.26}$$

Using the expressions above, we obtain

$$\int A(E,f)p(E)n(E+hf)\,dE \; = \alpha_b(f)\frac{c}{n_r(f)}\frac{\left(1 + \frac{f}{n_r}\frac{dn_r}{df}\right)^{-1}}{e^{(hf-q_eV)/kT}-1} \tag{3.27}$$

The radiative recombination rate refers to the frequency of recombination events where photons are emitted, reckoned as the number of these events per unit volume and time. This rate is proportional to the product of electron and hole concentrations $R_r = B_r np$, where the proportionality constant is the radiative recombination coefficient B_r [48]. Hence,

$$B_r(f)np = \int \left(\frac{dn(E)}{dt}\right)_{spon} dE \; = \int A(E,f)g_{ph}(f)p(E)n(E+hf)\,dE \tag{3.28}$$

Combining the last two equations, we obtain the radiative recombination coefficient

$$B_r(f) = \frac{\alpha_b(f)}{np}\frac{c}{n_r(f)}\rho(f)\left(1 + \frac{f}{n_r}\frac{dn_r}{df}\right)^{-1} \tag{3.29}$$

This can be expressed in terms of the photon energy as

$$B_r(E) = \alpha_b(f)\frac{n_r^2(f)}{c^2}\frac{8\pi E^2}{h^3 np}\frac{1}{e^{(hf-q_eV)/kT}-1} \tag{3.30}$$

The extra factor of h in the denominator comes from the fact that $df\rho_f(f) = dE\rho_E(E)$, giving

$$\rho_E(E) = \rho_f(E/h)/h \tag{3.31}$$

where the subscripts f and E indicate the type of the argument of the radiation spectrum.

In a non-degenerate semiconductor

$$q_eV < E_g < hf = E \quad , \quad e^{(E-q_eV)/kT} \gg 1 \quad , \quad np = n_i^2(V)e^{q_eV/kT} \tag{3.32}$$

where $n_i(V) = n_{i0}e^{\Delta E_g(V)/(2kT)}$ is the intrinsic concentration corrected with respect to the bandgap narrowing effect [49]. Therefore, we can approximate

$$B_r(f) \approx \alpha_b(f)\frac{n_r^2(f)}{c^2}\frac{8\pi f^2}{n_i^2(V)}e^{-hf/kT} \tag{3.33}$$

as stated in [51] and [29], This can be expressed in terms of the photon energy $E = hf$ as

$$B_r(f) \approx \alpha_b(E)\frac{n_r^2(E)}{c^2}\frac{8\pi E^2}{h^3n_i^2}e^{-E/kT} \tag{3.34}$$

The function $B_r(E)$ is proportional to the probability that in a radiative recombination event, a photon of energy E will be emitted. The net radiative recombination coefficient is

$$B_r = \int_0^\infty B_r(E)\,dE \tag{3.35}$$

If the parasitic absorption were not in operation, we could calculate the effective recombination coefficient by multiplying Equation (3.34) by the probability of escape, $P_{esc} = 1 - P_{reabs}$ and integrating it over the energy. However, because only the photons that undergo band-to-band transitions of the electrons are recycled through reabsorption, the reabsorption probability P_{reabs} needs to be multiplied by the probability of the band-to-band transition during that event. As a result, the effective recombination coefficient is modified accordingly

$$B_{r,eff} = \int_0^\infty B_r(E)\left(1 - \frac{\alpha_b(E)}{\alpha(E)} P_{reabs}(E)\right) dE \tag{3.36}$$

and this can be expressed as [29] , [52] :

$$B_{r,eff} = (1 - P_{PR}) B_r \tag{3.37}$$

and the net photon recycling probability is [29] , [52]

$$P_{PR} = B_r^{-1} \int_0^\infty B_r(E) \frac{\alpha_b(E)}{\alpha(E)} P_{reabs}(E)\, dE \tag{3.38}$$

3.4 Ideal solar cell model

3.4.1 Solar cell architecture

The design of the solar cell considered in this thesis and its energy band diagram is shown schematically in Figure 3.1(a) and (b). Generation of the electron-hole pairs

proceeds in the i-Si region of width L sandwiched between thin n- and p-type Si layers, which collect the photogenerated charge carriers of the same polarity. The outer surfaces of the p- and n-Si layers are made rough for Lambertian trapping of the incident photons. The bottom layer is a metal (M) electrode forming an ideal ohmic contact with the p-Si layer. The top layer is an antireflecting coating (ARC) to make sure that the incident photons enter the cell without optical losses. It is combined with a transparent conducting oxide (TCO) layer for current collection.

In real solar cells, the front and back surfaces are not Lambertian; rather, they are textured [53, 54]. Lambertian surfaces assumed here can be viewed as a mathematical limit of high texturing, at which surface reflection in all directions becomes equally probable.

The solar cell design shown in Figure 3.1 is reminiscent of the silicon solar cells with the efficiency approaching [55] and exceeding 25 % [27, 28, 56, 57], see [53, 54] for review. This value is already quite close to the limit efficiency of Si solar cells, evaluated to be about 29.5 % [29, 32, 47]. In those solar cells, the electron-hole pair generation proceeds in a relatively weakly doped Si base region sandwiched between two heavily doped n^+- and p^+-Si layers. For instance, the doping level in the base region of the solar cell with the record efficiency of above 26 % [27, 57] is $1.5 \cdot 10^{15}\,\mathrm{cm}^{-3}$, as inferred from the resisitivity value of $3\,\Omega\,\mathrm{cm}$.

The reason why intrinsic rather than doped silicon is chosen as a base material

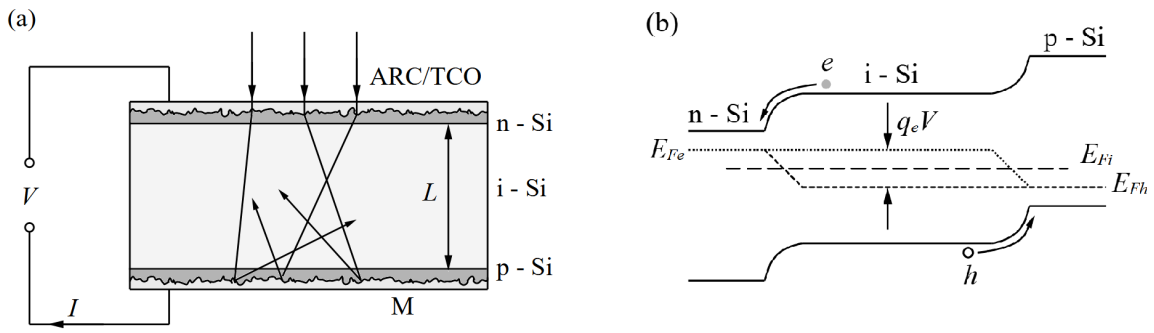

Figure 3.1: (a) Solar cell model considered in this thesis. (b) Energy band diagram of this solar cell, showing the Fermi energy E_{Fi} in i-Si and electron and hole quasi-Fermi energies E_{Fe} and E_{Fh}; their difference equals the voltage across the cell, $E_{Fe} - E_{Fh} = q_eV$. The photogenerated electrons and holes are collected by the n-Si and p-Si layers, respectively.

is that the recombination rate is minimal in an intrinsic semiconductor. Indeed, let us consider radiative recombination, which proceeds with the rate $U_r = B_r(np - n_0 p_0)$. Keeping in mind that the non-equilibrium concentrations are $n = n_0 + \Delta n$ and $p = p_0 + \Delta n$, the above equation can be rewritten as

$$U_r = B_r \left(n_0 + n_i^2 / n_0 + \Delta n \right) \Delta n \,, \tag{3.39}$$

where we expressed hole equilibrium concentration in terms of the electron concentration according to the mass action law $p_0 = n_i^2 / n_0$. At a fixed excess carrier concentration Δn, the radiative recombination rate (3.39) can be minimized with respect to the equilibrium electron concentration n_0, which is directly related to the doping level by [10]

$$n_0 = \frac{N_d - N_a}{2} + \sqrt{\frac{(N_d - N_a)^2}{4} + n_i^2} \,. \tag{3.40}$$

It immediately follows that U_r is minimal when $n_0 = n_i$, i.e. when the semiconductor is intrinsic.

A similar reasoning applies to Auger recombination with the rate

$$U_A = C_e(n^2 p - n_0^2 p_0) + C_h(np^2 - n_0 p_0^2) \,, \tag{3.41}$$

where C_e and C_h are Auger coefficients [10]. More precisely, minimization of U_A is achieved at the optimal doping level that depends on the ratio of the Auger coefficients C_e / C_h; however, if this ratio equals to 1, the optimal doping level again

turns out to be zero. In silicon, as in most semiconductors, both coefficients have similar values, which still implies a negligibly small doping level of the same order of magnitude as the intrinsic concentration n_i.

3.4.2 Photoconversion parameters

When the thickness of the solar cell is much smaller than the diffusion length,

$$L \ll \sqrt{D\tau} \tag{3.42}$$

where D is the ambipolar diffusion coefficient and τ is the average lifetime, we can use thin-base approximation, within which the excess carrier concentration Δn is taken to be constant in the base region. This approximation was originally introduced by Green [58], and is used extensively to model high-efficiency solar cells [29, 32, 47, 57]. Indeed, the typical recombination time value is of the order $\tau \sim 1\,\mathrm{ms}$ [57], and the diffusion coefficient $D \sim 10\,\mathrm{cm}^2/\mathrm{s}$, giving the diffusion length of the order of 1 mm. It is an order of magnitude higher than the optimal base thickness of about 100 μm, see below.

With the expression (3.38) for photon recycling probability, we now reassess the maximal efficiency of an i-Si solar cell within the thin-base approximation, assuming the current density to be

$$J(V) = J_L(V) - q_e L \Delta n(V) \left(\frac{1}{\tau_r} + \frac{1}{\tau_A} \right) . \tag{3.43}$$

The spectral flux density $\Phi(E)$ is taken to be the AM1.5G spectrum and its product with the absorptance corrected for interband transitions is integrated to find the light-generated current

$$J_L = q_e \int dE\, \Phi(E)\, \frac{\alpha_b(E)}{\alpha(E)}\, A(E)\,, \tag{3.44}$$

$\Delta n(V) = n(V) - n_{i0}$ is the excess carrier concentration, the radiative recombination time is found as

$$\tau_r^{-1} = (1 - P_{PR})(2n_{i0} + \Delta n)\, B_r\,, \tag{3.45}$$

and Auger lifetime τ_A is taken from the most recent evaluation [31]

$$\tau_A = \frac{\Delta n}{C_e g_e (n^2 p - n_0^2 p_0) + C_h g_h (n p^2 - n_0 p_0^2)} = \frac{\Delta n}{\Delta R_{Auger}} \tag{3.46}$$

where C_e and C_h are Auger coefficients and the correction factors g_e and g_h are functions of charge carrier density and describe the transition between pronounced Coulomb enhancement for low carrier concentrations to its absence at higher concentrations [31]. The maximal power condition $d(JV)/dV = 0$ yields the voltage V_m and the current density J_m, which then give the cell efficiency

$$\eta = \frac{J_m V_m}{\int dE\, E\, \Phi(E)}\,. \tag{3.47}$$

3.5 Results and discussion

3.5.1 Exact vs. approximate expressions for reabsorbption probability

When an incident photon is absorbed in the semiconductor material of a solar cell, it excites an electron from the valence band to the conduction band. This creates an electron-hole pair. However, a non-negligible probability exists that this excited electron will recombine with a hole in the valence band, emitting a photon with similar energy. This reabsorption process, often termed photon recycling, can lead to a reduced effective path length of photons within the absorber material, limiting the overall absorption efficiency and degrading solar cell performance.

Several factors influence photon reabsorption probability. Notably, the bandgap of the semiconductor material plays a critical role. A narrower bandgap results in a higher reabsorption probability, as many photons possess energy levels suitable for exciting electrons across the bandgap. Furthermore, the optical properties of the material, such as its refractive index and absorption coefficient, affect the reabsorption probability. Various optical structures, such as antireflective coatings and light-trapping techniques, affect the probability of photon escape and reabsorption in the solar cell.

It is instructive to compare the exact formula, Equation (2.26), with the approx-

imations for the reabsorption probability used in the literature. The first one, employed by Richter et al. [29], sets

$$P_{reabs,1} = A_{weak\,abs.} \tag{3.48}$$

with $A_{weak\,abs.}$ given by Equation (2.11). This approximation neglects the dependence of the reabsorption probability on the position x of the origin of a photon, the isotropy of the initial angular distribution, and assumes that all photons are weakly absorbed.

The second approximation, used in [30], replaces the approximate expression for the absorptance with the exact one from Equation (2.8):

$$P_{reabs,2} = A\ . \tag{3.49}$$

Finally, a more elaborate approximate expression was derived recently by Fell et al. [31]:

$$P_{reabs,3} = 1 - \frac{1 - T_L}{\ln T_L^{-1}} \left(1 - \frac{(1 - T_L)(1 - 1/(2n_r^2))}{1 - T_L(1 - 1/(2n_r^2))} \right)\ , \tag{3.50}$$

where T_L is given by Equation (2.14).

The relative error of each approximation is calculated as

$$100\,\% \times (P_{reabs,i} - P_{reabs})/P_{reabs} \tag{3.51}$$

with $i = 1,2,3$. Its sign indicates whether the ith approximation overestimates or underestimates the reabsorption probability.

All three approximate formulas, as well as the exact result, Equation (2.26), depend on two non-dimensional parameters: the refractive index n_r and the product αL. We have found numerically that increasing n_r results in a better accuracy of all three approximations. Therefore, we plot P_{reabs} vs. αL for a low value $n_r = 1.5$ and for the value $n_r = 3.5$ typical for Si in Figure (3.2) and the relative error of each approximation in Figures (3.3(a) and (b)).

It can be concluded from Figure (3.2) that all three approximations qualitatively agree with the exact curve. In particular, at high values of $\alpha L \gg 1$, all approximations give $P_{reabs} \to 1$ with the relative error tending to zero. In the opposite limit $\alpha L \ll 1$, all three approximations underestimate P_{reabs} with the relative error increasing in magnitude with decreasing αL. However, this error should play no role in the practical applications, because P_{reabs} itself tends to 0 at small αL.

Out of all three approximations, it is the second one, $P_{reabs,2}$, that deviates the most from the exact curve, while the most recent Equation (3.50) and the simplest expression, Equation (3.48), have about the same accuracy, see Figures (3.3(a) and (b)). In particular, for $n_r = 1.5$, the deviation of the simplest approximation, Equation (3.48), from the exact curve has the peak value of about 7 % at $\alpha L = 0.07$ and is similar to the error of the formula, Equation (3.50), at the same αL. For a more realistic refractive index value of 3.5, this approximation overestimates the reabsorption probability by only 0.5 % at $\alpha L = 0.03$, whereas Equation (3.50) underestimates

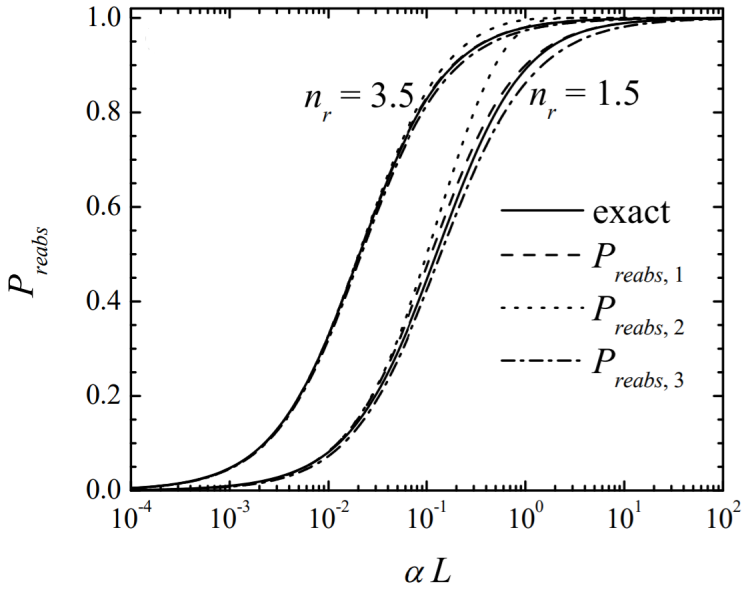

Figure 3.2: The probability of photon reabsorption as a function of the product of the absorption coefficient and the thickness of a slab with the refractive index $n_r = 1.5$ and $n_r = 3.5$. Solid line: exact result Equation (2.26). The dashed line, the dotted line, and the dash-dotted lines are obtained with the approximations (3.48), (3.49), and (3.50), respectively. The relative error of each approximation, whose number is indicated near each curve, is shown in panel

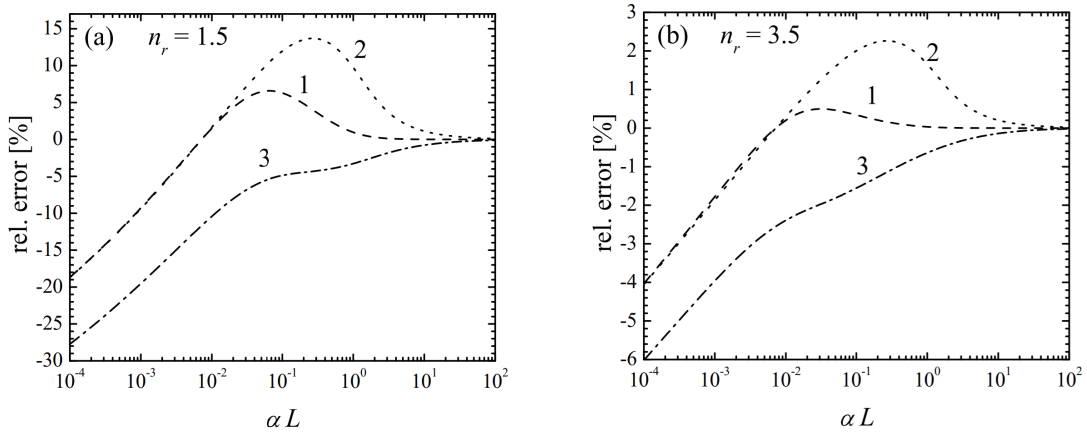

Figure 3.3: The relative error of each approximation, whose number is indicated near each curve, is shown in panel (a) for $n_r = 1.5$ and in panel (b) for $n_r = 3.5$.

it by 2 % at this αL value.

The spectral dependence of the reabsorption coefficient of a Si slab of 100 μm thickness at 300 K is presented in Figure (3.4) with the relative error of each approximation shown in the inset of this figure. Again, it is seen that the simplest approximation, Equation (3.48), is the most accurate one, as it agrees with the exact curve to within 0.05 % at $\lambda < 1\,\mu$m and overestimates P_{reabs} by only 0.5 % at the wavelength corresponding to the bandgap energy in Si. The other two approximations, Equation (3.49) and (3.50), perform reasonably well, but have a significantly higher inaccuracy within 2 %.

The quite good agreement of all three approximations with the exact expres-

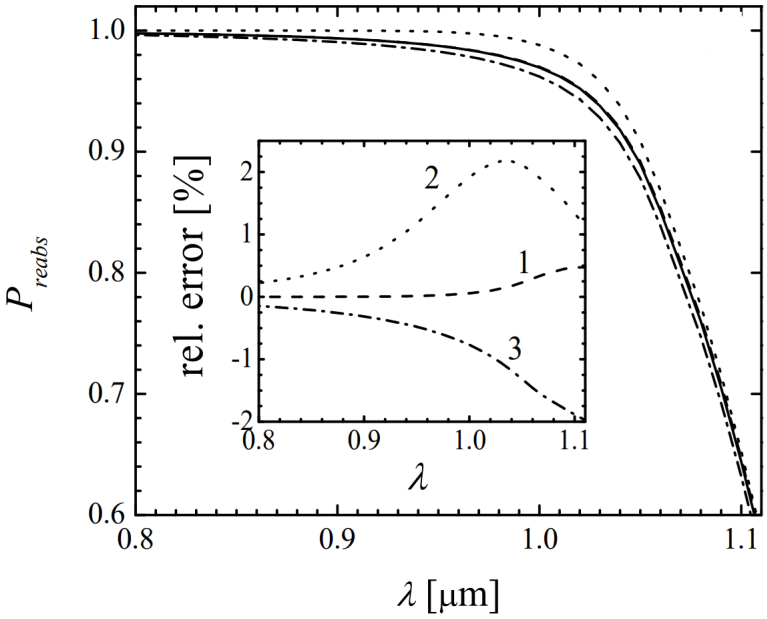

Figure 3.4: Spectral dependence of the reabsorption probability in a Si slab of thickness $L = 100\,\mu$m at 300 K with the relative error of each approximation shown in the inset.

sion may be attributed to the fact that all of them have correct asymptotic limits $P_{reabs} \to 0$ and 1 at low and high αL, respectively. In the intermediate αL range, the photons produced in the recombination events have a decent chance to reach the front surface and get reflected from it. From that point on, their reabsorption probability equals absorptance, which is the basis of all three approximations, Equations ((3.48)-(3.50)). The high accuracy of the simplest approximation, Equation (3.48), is nevertheless surprising, as its derivation involves more simplifying assumptions than the other two approximations do.

It is known from studies of photon recycling in thin film GaAs cells [59] that the quality of the reflector has a decisive impact on the potential benefit from photon recycling. This can be taken into account by introducing an additional model parameter, the reflection coefficient $r_B(\lambda)$ of the back surface as a function of the wavelength. To be consistent with the assumption of Lambertian scattering, it should be assumed independent of the photon angle of incidence.

It is possible to derive the photon reabsorption probability within the so generalized model. Here, given the high accuracy of the simplest approximation, Equation (3.48), obtained in the special case $r_B = 1$, we would like to propose a simpler option. It consists in correcting the escape probability Equation (2.4) with respect to absorption by the back reflector

$$p_e = n_r^{-2} + 1 - r_B \tag{3.52}$$

and modifying the Tiedje-Yablonovitch formula, Equation (2.8), accordingly. The resulting approximation, namely,

$$P_{reabs} = \left(1 + \frac{1 + n_r^2(1 - r_B)}{4n_r^2 \alpha L}\right)^{-1}, \tag{3.53}$$

is expected to be accurate to within 0.5 % for most practical purposes.

3.5.2 Photon recycling probability

Figure 3.5(a) shows the behavior of the photon recycling probability P_{PR} of an intrinsic Si cell as a function of its thickness L at 25 °C according to Equations ((2.26) and (3.38)). In the calculations, the most recent optical data of Si were used [60]. It was assumed that parasitic absorption stems entirely from the free carriers, and so α_p was parameterized according to [61].

The free-carrier absorption coefficient α_p increases with the excess concentration of charge carries, which is given by the generalized mass action law (3.1). The electron and hole concentrations in an intrinsic semiconductor are equal to each other, $n = p = n_i(V) + \Delta n(V)$, where the intrinsic concentration slightly changes with voltage due to the bandgap narrowing, see Equation (3.2), and

$$\Delta n(V) = n_i(V)(e^{qV/(2kT)} - 1) \tag{3.54}$$

is the excess concentration that follows from Equation (3.1). Hence, due to the term $\alpha_b/(\alpha_b + \alpha_p)$ in Equation (3.38), the photon recycling probability decreases with V.

Table 3.1: Expansion coefficients in Equation (3.56)

	a_0	a_1	a_2	a_3	a_4	a_5	a_6	a_7
$P_0(L)$	0.06076	0.04689	0.01409	0.00134	$-1.4903 \cdot 10^{-4}$	$-2.2623 \cdot 10^{-5}$	$-2.4513 \cdot 10^{-6}$	$4.283 \cdot 10^{-7}$
$V_0(L)$	1.01518	-0.00817	-0.002	$-6.974 \cdot 10^{-5}$	$4.746 \cdot 10^{-5}$	$9.547 \cdot 10^{-7}$	$-3.762 \cdot 10^{-7}$	0
$\Delta V(L)$	0.05487	$4.671 \cdot 10^{-4}$	$2.333 \cdot 10^{-4}$	$-9.221 \cdot 10^{-6}$	$-8.915 \cdot 10^{-6}$	$1.746 \cdot 10^{-6}$	$-9.26 \cdot 10^{-8}$	0

However, this decrease is insignificant for $V < 0.75\,\mathrm{V}$, i.e. for the voltages below the open-circuit voltage of a Si solar cell.

The relative error or each approximation at $V = 0$ is shown in Figure (3.5(b)). It is seen that the most accurate approximation is the simplest one, given by Equations ((3.48), (2.8)) with the accuracy better than 0.3 %. The other two approximations, Equations ((3.49) and (3.50)), are of comparable quality. As the voltage is increased, all three relative error curves get shifted up, so that at $V = 0.75\,\mathrm{V}$, the approximation of Equation (3.50), becomes the most accurate out of all three, see Figure (3.5(c)).

The photon recycling probability as a function of voltage for different cell thicknesses is shown in Figure (3.6(a)). For most practical purposes, it can be fitted with a sigmoid function

$$P_{PR}(V,L) = \frac{P_0(L)}{1 + e^{(V - V_0(L))/\Delta V(L)}}\,. \tag{3.55}$$

The accuracy of this fit is better than 0.5 %. At the standard testing temperature $T = 25^{\circ}\mathrm{C}$,the reabsorption probability at $V \ll V_0$ can be approximated with a seventh-

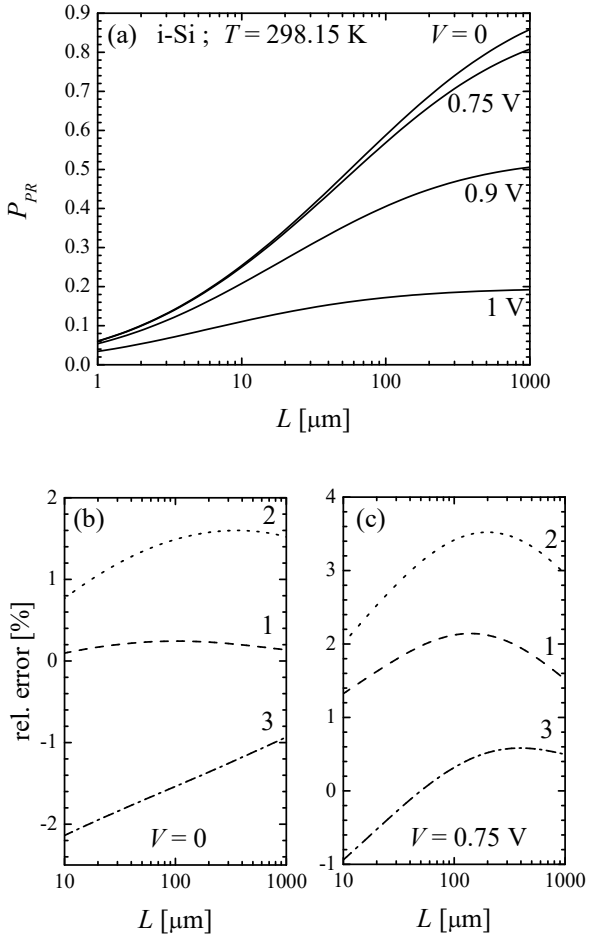

Figure 3.5: (a) The photon recycling probability (2.26), (3.38) as a function of an i-Si cell thickness at different values of the voltage across the cell, as indicated near each solid curve. (b) The relative error of the photon recycling probability obtained with Equation (3.38) and the approximations (3.48) (dashed line 1), (3.49) (dotted line 2), and (3.50) (dash-dotted line 3) at $V = 0$ and (c) $V = 0.75$.

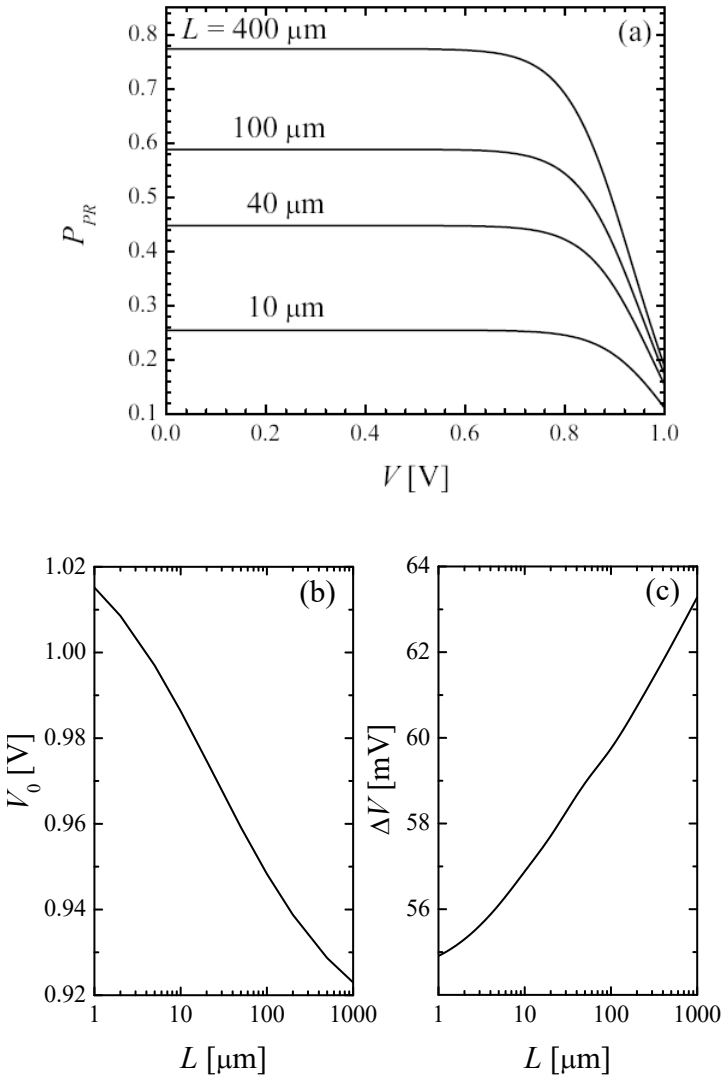

Figure 3.6: (a) Photon recycling probability as a function of voltage across the cell at different values of the cell thickness at $T = 298.15\,\mathrm{K}$. (b) Thickness dependence of the parameters V_0 and (c) ΔV from the fitting formula (3.55) corresponding to the case of i-Si.

order polynomial in $x = L/(1\mu\text{m})$ as

$$f(L) = \sum_{k=0}^{7} a_k x^k \tag{3.56}$$

with $f(L) = P_0(L)$, $V_0(L)$, or $\Delta V(L)$. The coefficients of this expansion are given in Table 3.1. This approximation is accurate in the range $100\,\text{nm} < L < 1\,\text{mm}$. It also applies to the case of doped Si to a reasonable accuracy, as long as the charge carrier concentration does not exceed about $10^{16}\,\text{cm}^{-3}$; at higher Δn values, the Auger recombination time is so short that the diffusion length becomes comparable to the cell thickness, which implies the breakdown of the thin-base approximation.

Note that the parameters V_0 and ΔV depend very weakly on the cell thickness, see Figures (3.6 (b) and (c)), which shows that a change of L by a thousand times results in their variation by less than 10 % and less than 15 %, respectively. In view of the fact that at $V = 0$ the factor $e^{-V_0(L)/\Delta V(L)}$ in the denominator of Equation (3.55) is negligible, the upper curve in Figure (3.6(a)) is just $P_{PR}(0, L) = P_0(L)$ to a very high accuracy.

3.5.3 Maximal efficiency of a Si solar cell

The cell efficiency as a function of thickness at 25°C is shown in Figure (3.7). L_m is the thickness at the maximum efficiency, η_m is the maximum efficiency, and V_{OC} is the open-circuit voltage which is the difference of electrical potential between two terminals of an electronic device when disconnected from any circuit. J_{SC}

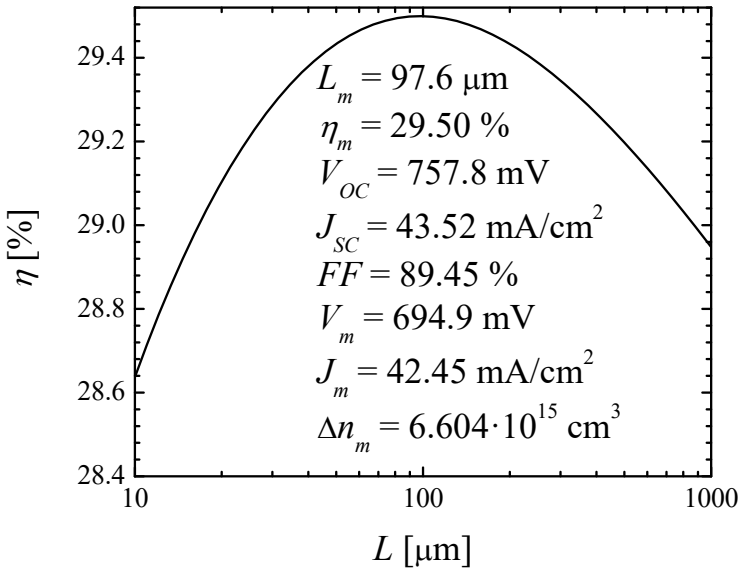

Figure 3.7: Thickness dependence of the photoconversion efficiency of an ideal solar cell with an i-Si base at 298.15 K. The inset shows the values of the thickness at the efficiency maximum, the maximal efficiency, the open circuit voltage, the short circuit current density, the fill factor, voltage, current density, and the excess carrier concentration at the maximal output power.

is the short-circuit current density at zero voltage, V_m is maximum voltage, J_m is maximum current density and Δn_m is excess carrier concentration at maximum power. FF or fill factor is the ratio of the actual maximum obtainable power to the product of short circuit current and open circuit voltage

$$FF = \frac{J_m V_m}{J_{SC} V_{OC}}. \tag{3.57}$$

The non-monotonic behaviour of efficiency with the cell thickness has been reported in similar theoretical works [20, 29, 47], but we are unaware of analogous experimental studies. This dependence can be understood as resulting from the competition of two effects. At small thickness, the photons that enter the cell have a very high probability of escape, and this η should decrease as L is made smaller. On the other hand, at large thickness, practically all incident photons are absorbed by the material. However, the concentration of the excess electron-hole pairs should decrease with L at a constant generation rate, $\Delta n \propto 1/L$. Therefore, also the photoconversion efficiency should get smaller as L is increased above the optimal value.

The efficiency maximum value of 29.5 % is found at the cell thickness of 97.6 μm; other parameters that characterize the current-voltage curve are indicated in the inset of Figure (3.7). The maximal efficiency reported here is practically the same as calculated in [20].

The obtained maximal efficiency exceeds the most recent estimate [31] by 0.1 %-abs. This difference may be attributed to the fact that the authors of [31] performed numerical integration of the stationary diffusion equation using Quokka3 software. On the other hand, the thin-base approximation takes the excess carrier concentration as uniform within the base region and therefore neglects the transport losses of the photogenerated electron-hole pairs.

We note that the approximation of uniform excess concentration is consistent with the assumption of uniform photon production inside the base. On the other hand, correct incorporation of photon recycling effect in a model with non-uniform concentration profile is a highly non-trivial task, as the electron-hole pair generation rate at a given point x would have to include an extra term that depends on the integral of the radiative recombination rate over the whole cell:

$$G_{PR}(x) = \int_0^L dx' \, \frac{\Delta n(x')}{\tau_r(x')} \, P_{PR}(x|x') \, , \tag{3.58}$$

where $P_{PR}(x|x')$ is the conditional probability for a photon produced at a point x' to be recycled at a point x. But without performing this calculation, we can reasonably expect that the effect of this extra term would be to reduce the non-uniformity of $\Delta n(x)$. The reason is that radiative recombination proceeds at a higher rate in the region of high excess carrier concentration, while the so produced photons are more likely to get recycled in the region of low carrier concentration.

Chapter 4

Conclusions

This research delves into how Lambertian surfaces play a crucial role in shaping how photons move within solar cell structures. The study uncovers a significant way to boost solar cell efficiency by examining how these ideal scatterers influence photon movement. Using reflective surfaces strategically helps capture escaping photons, absorbing them again within the semiconductor material, creating electron-hole pairs. This process of reabsorption and reuse offers an exciting avenue to significantly increase the overall efficiency of solar cells, pushing forward advancements in renewable energy technologies.

Moreover, the study emphasizes the practical usefulness of the thin-base approximation method in understanding how photons recycle within solar cells. This analytical approach simplifies how we understand this process and gives us a clear

view of how reabsorption mechanisms impact solar cell efficiency. The insights from this study lay the groundwork for improving how we analyze and model solar cell designs to make them perform even better.

This study focused on deriving an analytical expression that explicitly calculated the probability of reabsorption and recycling of photons generated during a radiative recombination event within a semiconductor slab. What is intriguing is that our results remain remarkably accurate even when accounting for the assumption of ideal Lambertian scatterers on both slab surfaces. We evaluated various approximations to estimate reabsorption probability against our exact results, demonstrating a remarkable level of precision with deviations within a narrow range of just a few percentage points.

Particular interest is the discovery that the simplest approximation sourced from [29], which involves aligning P_{reabs} with the absorptance asymptotic formula from [39], emerged as the most accurate among the methods evaluated. This seemingly straightforward approximation surprisingly stood out for its precision, showcasing the intriguing interplay between simplicity and accuracy in our research.

Furthermore, our investigation brought to light an interesting observation regarding the role of free carrier absorption in photon recycling. Contrary to some expectations, our findings indicate that free carrier absorption only influences pho-

ton recycling, particularly at voltages operating below the open-circuit threshold. This understanding enriches our comprehension of the complex mechanisms governing photon recycling within semiconductor slabs.

Moreover, operating within the framework of the thin-base approximation, our study extended its exploration to determine the efficiency of a silicon solar cell. Our rigorous analysis unveiled an impressive limiting efficiency of 29.5 % for such a solar cell configuration, specifically observed at a thickness of 98 μm. These findings underscore the precision of our analytical approach and hold significant implications for advancing solar cell technology.

Bibliography

[1] Abdelhalim Zekry, Ahmed Shaker, and Marwa Salem. Solar cells and arrays: Principles, analysis and design. In *Advances in Renewable Energies and Power Technologies*, volume 1, pages 3–56. Elsevier, 2018.

[2] Vitezslav Benda. Photovoltaics, including new technologies (thin film) and a discussion on module efficiency. In Trevor M. Letcher, editor, *Future Energy*, pages 375–412. Elsevier, 3rd edition, 2020.

[3] Franco Gaspari and Simone Quaranta. PV materials. In Ibrahim Dincer, editor, *Comprehensive Energy Systems*, pages 117–149. Elsevier, Oxford, 2018.

[4] Stephen J. Fonash. Structures, materials, and scale. In Stephen J. Fonash, editor, *Solar Cell Device Physics (Second Edition)*, pages 67–120. Academic Press, Boston, 2nd edition, 2010.

[5] Michael Mauk, Paul Sims, James Rand, and Allen Barnett. Thin silicon solar

cells. In Augustin McEvoy, Luis Castañer, and Tom Markvart, editors, *Solar Cells*, pages 115–156. Elsevier, 2nd edition, 2013.

[6] Yilin Li and Wen-Ji Dong. Estimating the theoretical limit of the power conversion efficiency of a luminescent solar concentrator device from the perspective of Shockley-Queisser limit. In *2015 IEEE 42nd Photovoltaic Specialist Conference (PVSC)*, pages 1–3, 2015.

[7] A.R. Zanatta. The Shockley–Queisser limit and the conversion efficiency of silicon-based solar cells. *Results in Optics*, 9:100320, 2022.

[8] Xufeng Wang, Mohammad Ryyan Khan, Muhammad A. Alam, and Mark Lundstrom. Approaching the Shockley-Queisser limit in GaAs solar cells. In *2012 38th IEEE Photovoltaic Specialists Conference*, pages 002117–002121, 2012.

[9] Genichi Hatakoshi and Kenichi Iga. Consideration of equilibrium condition in Shockley-Queisser limit for solar cell efficiency. In *2017 22nd Microoptics Conference (MOC)*, pages 104–105, 2017.

[10] M. Evstigneev. *Introduction to semiconductor physics and devices*. Springer International Publishing, 2022.

[11] P.T. Landsberg. Semiconductor physics — recombination processes. In

Robert D. Guenther, editor, *Encyclopedia of Modern Optics*, pages 21–29. Elsevier, Oxford, 2005.

[12] Giso Hahn and Sebastian Joos. State-of-the-art industrial crystalline silicon solar cells. In Gerhard P. Willeke and Eicke R. Weber, editors, *Advances in photovoltaics*, volume 90 of *Semiconductors and Semimetals*, pages 1–72. Elsevier, 2014.

[13] E.F Schubert and T. Gessmann. Light emitting diodes. In Franco Bassani, Gerald L. Liedl, and Peter Wyder, editors, *Encyclopedia of condensed matter physics*, pages 102–111. Elsevier, Oxford, 2005.

[14] In Robert Triboulet and Paul Siffert, editors, *CdTe and related compounds; Physics, defects, hetero- and nano-structures, crystal growth, surfaces and applications*, European Materials Research Society Series, pages 5–97. Elsevier, Amsterdam, 2010.

[15] H. Yu, C. Xin, Q. Zhang, M.I.B. Utama, L. Tong, and Q.H. Xiong. II–VI compound semiconductor nanowires: Optical properties and nanophotonics. In Jordi Arbiol and Qihua Xiong, editors, *Semiconductor nanowires*, Woodhead Publishing Series in Electronic and Optical Materials, pages 29–69. Woodhead Publishing, 2015.

[16] Valerio Piazza, Lorenzo Mancini, Hung-Ling Chen, Stéphane Collin, and

Maria Tchernycheva. Nanoscale analyses applied to nanowire devices. In Sudha Mokkapati and Chennupati Jagadish, editors, *Nanowires for energy applications*, volume 98 of *Semiconductors and Semimetals*, pages 231–319. Elsevier, 2018.

[17] P. Blood. Principles of semiconductor lasers. In Alexei Baranov and Eric Tournié, editors, *Semiconductor Lasers*, Woodhead Publishing Series in Electronic and Optical Materials, pages 3–55. Woodhead Publishing, 2013.

[18] Annamraju Kasi Viswanath. Surface and interfacial recombination in semiconductors. In Hari Singh Nalwa, editor, *Handbook of surfaces and interfaces of materials*, pages 217–284. Academic Press, Burlington, 2001.

[19] M.J. Kerr and A. Cuevas. Recombination at the interface between silicon and stoichiometric plasma silicon nitride. *Semicond. Sci. Technol.*, 17:166–172, 2002.

[20] Boris A. Veith-Wolf, Sören Schäfer, Rolf Brendel, and Jan Schmidt. Reassessment of intrinsic lifetime limit in n-type crystalline silicon and implication on maximum solar cell efficiency. *Solar Energy Materials and Solar Cells*, 186:194–199, 2018.

[21] Bernd Steinhauser, Tim Niewelt, Armin Richter, Rebekka Eberle, and Martin C. Schubert. Extraordinarily high minority charge carrier lifetime observed in crystalline silicon. *Solar RRL*, 5(11):2100605, 2021.

[22] Taro Hayakawa, Motoharu Miyamoto, Koichi Koyama, Keisuke Ohdaira, and Hideki Matsumura. Extremely low recombination velocity on crystalline silicon surfaces realized by low-temperature impurity doping in Cat-CVD technology. *Thin Solid Films*, 519(14):4466–4468, 2011.

[23] Yoh-Ichiro Ogita, Masayuki Tachihara, Yotaro Aizawa, and Naoyuki Saito. Ultralow surface recombination in p-Si passivated by catalytic-chemical vapor deposited alumina films. *Thin Solid Films*, 519(14):4469–4472, 2011.

[24] Koichi Koyama, Keisuke Ohdaira, and Hideki Matsumura. Excellent passivation effect of Cat-CVD SiN_x/i-a-Si stack films on Si substrates. *Thin Solid Films*, 519(14):4473–4475, 2011.

[25] Ch. Rajesh, M.R. Pramod, Sumati Patil, Shailaja Mahamuni, Shahaji More, R.O. Dusane, and S.V. Ghaisas. Reduction in surface recombination through hydrogen and 1-heptene passivated silicon nanocrystals film on silicon solar cells. *Solar Energy*, 86(1):489–495, 2012.

[26] Tim Niewelt, Wolfram Kwapil, Marisa Selinger, Armin Richter, and Martin C. Schubert. Long-term stability of aluminum oxide based surface passivation schemes under illumination at elevated temperatures. *IEEE Journal of Photovoltaics*, 7(5):1197–1202, 2017.

[27] Kunta Yoshikawa, Wataru Yoshida, Toru Irie, Hayato Kawasaki, Katsunori

Konishi, Hirotaka Ishibashi, Tsuyoshi Asatani, Daisuke Adachi, Masanori Kanematsu, Hisashi Uzu, and Kenji Yamamoto. Exceeding conversion efficiency of 26 % by heterojunction interdigitated back contact solar cell with thin film Si technology. *Solar Energy Materials and Solar Cells*, 173:37–42, 2017.

[28] Kenji Yamamoto, Kunta Yoshikawa, Hisashi Uzu, and Daisuke Adachi. High-efficiency heterojunction crystalline Si solar cells. *Japanese Journal of Applied Physics*, 57(8S3):08RB20, 2018.

[29] Armin Richter, Martin Hermle, and Stefan W. Glunz. Reassessment of the limiting efficiency for crystalline silicon solar cells. *IEEE Journal of Photovoltaics*, 3(4):1184–1191, 2013.

[30] Anatoly Sachenko, Vitaliy Kostylyov, Igor Sokolovskyi, and Mykhaylo Evstigneev. Effect of temperature on limit photoconversion efficiency in silicon solar cells. *IEEE Journal of Photovoltaics*, 10(1):63–69, 2020.

[31] T. Niewelt, B. Steinhauser, A. Richter, B. Veith-Wolf, A. Fell, B. Hammann, N.E. Grant, L. Black, J. Tan, A. Youssef, J.D. Murphy, J. Schmidt, M.C. Schubert, and S.W. Glunz. Reassessment of the intrinsic bulk recombination in crystalline silicon. *Solar Energy Materials and Solar Cells*, 235:111467, 2022.

[32] Mykhaylo Evstigneev and Faezeh Farahani. Photon recycling in a solar cell

with two Lambertian surfaces. *IEEE Journal of Photovoltaics*, 13(2):260–266, 2023.

[33] Matt Pharr, Wenzel Jakob, and Greg Humphreys. Reflection models. In Matt Pharr, Wenzel Jakob, and Greg Humphreys, editors, *Physically Based Rendering*, pages 507–568. Morgan Kaufmann, Boston, 3rd edition, 2017.

[34] Tom McReynolds and David Blythe. Lighting techniques. In Tom McReynolds and David Blythe, editors, *Advanced Graphics Programming Using OpenGL*, The Morgan Kaufmann Series in Computer Graphics, pages 317–359. Morgan Kaufmann, San Francisco, 2005.

[35] Michael Oren and Shree K. Nayar. Generalization of Lambert's reflectance model. In *Proceedings of the 21st Annual Conference on Computer Graphics and Interactive Techniques*, SIGGRAPH '94, page 239–246, New York, NY, USA, 1994. Association for Computing Machinery.

[36] R. Santbergen and R.J.C. van Zolingen. The absorption factor of crystalline silicon PV cells: A numerical and experimental study. *Solar Energy Materials and Solar Cells*, 92(4):432–444, 2008.

[37] Hao Lin, Jiajia Wang, Zilei Wang, Zhiyuan Xu, Pingqi Gao, and Wenzhong Shen. Edge effect in silicon solar cells with dopant-free interdigitated back-contacts. *Nano Energy*, 74:104893, 2020.

[38] M. J. Keevers and M. A. Green. Absorption edge of silicon from solar cell spectral response measurements. *Applied Physics Letters*, 66(2):174–176, 1995.

[39] T. Tiedje, E. Yablonovitch, G.D. Cody, and B.G. Brooks. Limiting efficiency of silicon solar cells. *IEEE Transactions on Electron Devices*, 31(5):711–716, 1984.

[40] Eli Yablonovitch. Statistical ray optics. *J. Opt. Soc. Am.*, 72(7):899–907, 1982.

[41] H. Saha, S.K. Datta, K. Mukhopadhyay, S. Banerjee, and M.K. Mukherjee. Influence of surface texturization on the light trapping and spectral response of silicon solar cells. *IEEE Transactions on Electron Devices*, 39(5):1100–1107, 1992.

[42] Rolf Brendel and Daphne Scholten. Modeling light trapping and electronic transport of waffle-shaped crystalline thin-film Si solar cells. *Applied Physics A*, 69:201–213, 1999.

[43] Martin A. Green. Lambertian light trapping in textured solar cells and light-emitting diodes: analytical solutions. *Progress in Photovoltaics: Research and Applications*, 10(4):235–241, 2002.

[44] Mark J. Kerr, Andres Cuevas, and Patrick Campbell. Limiting efficiency of crystalline silicon solar cells due to Coulomb-enhanced Auger recombination. *Progress in Photovoltaics: Research and Applications*, 11(2):97–104, 2003.

[45] W. Shockley and H.J. Queisser. Detailed balance limit of efficiency of p-n junction solar cells. *Journal of Applied Physics*, 32:510–519, 1961.

[46] M.A. Green. Limits on the open-circuit voltage and efficiency of silicon solar cells imposed by intrinsic Auger processes. *IEEE Transactions on Electron Devices*, ED-31:671–678, 1984.

[47] S. Schäfer and R Brendel. Accurate calculation of the absorptance enhances efficiency limit of crystalline silicon solar cells with Lambertian light trapping. *IEEE Journal of Photovoltaics*, 8:1156–1158, 2018.

[48] Peter Würfel. The chemical potential of radiation. *Journal of Physics C: Solid State Physics*, 15(18):3967, 1982.

[49] Andreas Schenk. Finite-temperature full random-phase approximation model of band gap narrowing for silicon device simulation. *Journal of Applied Physics*, 84(7):3684–3695, 10 1998.

[50] Orazio Svelto. *Principles of Lasers*. Springer US, 2010.

[51] Thorsten Trupke, Martin Green, Peter Wuerfel, Pietro Altermatt, A. Wang, J. Zhao, and Richard Corkish. Temperature dependence of the radiative recombination coefficient of intrinsic crystalline silicon. *Journal of Applied Physics*, 94:4930–4937, 2003.

[52] Andreas Fell, Tim Niewelt, Bernd Steinhauser, Friedemann D. Heinz, Martin C. Schubert, and Stefan W. Glunz. Radiative recombination in silicon photovoltaics: Modeling the influence of charge carrier densities and photon recycling. *Solar Energy Materials and Solar Cells*, 230:111198, 2021.

[53] Stefaan De Wolf, Antoine Descoeudres, Zachary C. Holman, and Christophe Ballif. High-efficiency silicon heterojunction solar cells: A review. *Green*, 2:7–24, 2012.

[54] Jingjing Liu, Yao Yao, Shaoqing Xiao, and Xiaofeng Gu. Review of status developments of high-efficiency crystalline silicon solar cells. *J. Phys. D: Appl. Phys.*, 51:123001, 2018.

[55] Mikio Taguchi, Ayumu Yano, Satoshi Tohoda, Kenta Matsuyama, Yuya Nakamura, Takeshi Nishiwaki, Kazunori Fujita, and Eiji Maruyama. 24.7 % record efficiency HIT solar cell on thin silicon wafer. *Applied Physics Letters*, 4, 2014.

[56] Daisuke Adachi, José Luis Hernández, and Kenji Yamamoto. Impact of carrier recombination on fill factor for large area heterojunction crystalline silicon solar cell with 25.1 % efficiency. *Applied Physics Letters*, 107(23), 12 2015. 233506.

[57] Kunta Yoshikawa, Hayato Kawasaki, Wataru Yoshida, Toru Irie, Katsunori Konishi, Kunihiro Nakano, Toshihiko Uto, Daisuke Adachi, Hisashi Kanematsu, Masanori Uzu, and Kenji Yamamoto. Silicon heterojunction solar cell

with interdigitated back contacts for a photoconversion effciency over 26 %. *Nature Energy*, 2:17032, 2017.

[58] M.A. Green. Limits on the open-circuit voltage and efficiency of silicon solar cells imposed by intrinsic auger processes. *IEEE 428 Trans. Electron Devices*, ED-31:671–678, 1984.

[59] Natasha Gruginskie, Federica Cappelluti, Gerard Bauhuis, Alberto Tibaldi, Gemma Giliberti, Peter Mulder, Elias Vlieg, and John Schermer. Limiting mechanisms for photon recycling in thin-film GaAs solar cells. *Progress in Photovoltaics: Research and Applications*, 29:379–390, 2021.

[60] Martin A. Green. Improved silicon optical parameters at 25°, 295 K and 300 K including temperature coefficients. *Progress in Photovoltaics: Research and Applications*, 30:164–179, 2022.

[61] Marc Rüdiger, Johannes Greulich, Armin Richter, and Martin Hermle. Parameterization of free carrier absorption in highly doped silicon for solar cells. *IEEE Transactions on Electron Devices*, 60:2156–2163, 2013.